Collisional excitation of interstellar PO($X^2\Pi$) by He: New *ab initio* potential energy surfaces and scattering calculations

François Lique*
LOMC - UMR 6294, CNRS-Université du Havre,
25 rue Philippe Lebon, BP 1123 - 76 063 Le Havre cedex, France

Izaskun Jiménez-Serra†
Astronomy Unit, School of Physics and Astronomy, Queen Mary University of London,
G. O. Jones Building, Mile End Road, London E1 4NS, UK

Serena Viti‡
Department of Physics and Astronomy, University College London, 132 Hampstead Road, London NW1 2PS, UK

Sarantos Marinakis§
Department of Chemistry and Biochemistry, School of Biological and Chemical Sciences,
Queen Mary University of London, Joseph Priestley Building, Mile End Road, London E1 4NS, UK
(Dated: September 10, 2017)

We present the first *ab initio* potential energy surfaces (PESs) for the PO($X\ ^2\Pi$)-He van der Waals system. The PESs were obtained using the open-shell partially spin-restricted coupled cluster approach with single, double and perturbative triple excitations [UCCSD(T)]. The augmented correlation-consistent polarized valence triple-zeta (aug-cc-pVTZ) basis set was employed supplemented by mid-bond functions. Integral and differential cross sections for the rotational excitation in PO-He collisions were calculated using the new PES and compared with results in similar systems. Finally, our work presents the first hyperfine-resolved cross sections for this system that are needed for accurate modelling in astrophysical environments.

I. INTRODUCTION

Although its solar and meteoritic abundance is rather low compared to other elements essential for life e.g. carbon, nitrogen, oxygen and sulfur [1], phosphorus is ubiquitous in the universe [2]. Phosphorus is believed to be synthesised both in the cores of massive stars and during supernovae explosions [3]. In the interstellar medium (ISM), phosphorus has been detected in the form of P^+ in diffuse clouds [4] and in molecular form mainly in circumstellar gas around evolved stars. Phosphorus-bearing species detected in circumstellar envelopes include the HCP, PH_3, CP, CCP, PO, and PN molecules [5, 6]. Unfortunately, the gas phase chemistry of phosphorus is not well studied partly because some of these molecules are very toxic. Among these species, the PO radical (or phosphorus monoxide) is considered as a molecular species of prebiotic interest since it is an essential compound in the formation of the backbone of DNA.

Thanks to its high dipole moment (1.88 Debye [7]) and high-sensitivity instrumentation, PO has successfully been detected in space. In chronological order, Tenenbaum et al. [8] presented the first detection of PO in the supergiant star VY Canis Majoris (VY CMa), making the first observation of the P-O bond in space. PO was observed in the AGB star IK Tauri by De Beck et al. in 2013 [9], and in star-forming regions by Rivilla et al. [10] and Lefloch et al. [11]. In most cases, the measured PO/PN ratios are between 0.17 and 4.5. These ratios carry valuable information about the length of the pre-stellar collapse phase and depend on the density, temperature and abundances of the N and O atoms [11, 12].

The ground electronic state configuration of PO is $(1-4)\sigma^2 1\pi^4 (5-6)\sigma^2 2\pi^4 7\sigma^2 3\pi^1$, and therefore the ground electronic state is of $^2\Pi$ symmetry. The phosphorus monoxide is a Hund's case (a) radical in its lowest rovibrational levels in the ground electronic state, with the $^2\Pi_{1/2}$ spin-orbit state being lower than the $^2\Pi_{3/2}$ as shown in Fig. 1. The lower and higher spin-orbit manifolds will be denoted hereafter as F_1 and F_2, respectively. Each rotational level j of PO is further split into two Λ-doublet levels, which are labelled e and f (Fig. 1). When the sign of the wavefunction of a given level remains the same under space-fixed inversion operator, the level has positive parity, $p = 1$. The e/f levels have parity $\pm(-1)^{(j-1/2)}$. All series of levels in which the electronic wavefunction at high j is symmetric or antisymmetric with respect the reflection of the spatial coordinates of the electrons in the plane of rotation are designated as A' or A'', respectively. For PO, the eF_1 and fF_2 levels are of A' parity, and the fF_1 and eF_2 of A'' parity. We note that the Λ-doublet splitting is very small, especially for the higher spin-orbit manifold. In addition, the ^{31}P, which is the only stable isotope of phosphorus, possesses a non-zero nuclear spin ($I = 1/2$), which couples with $\vec{j}$ resulting in a splitting of each Λ-doublet level into two

* francois.lique@univ-lehavre.fr
† i.jimenez-serra@qmul.ac.uk
‡ sv@star.ucl.ac.uk
§ s.marinakis@qmul.ac.uk

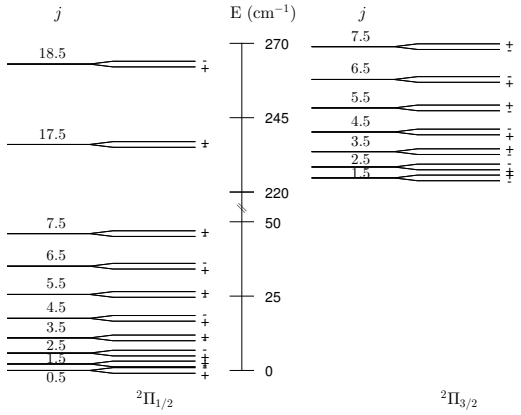

FIG. 1: Rotational energy levels of the electronic and vibrational ground state of PO. The zero reference energy is defined for the lowest PO rotational level (Ω = 0.5, j = 0.5e). The levels are labeled by total angular momentum of PO, and parity p. The energy difference between the Λ-doublet components is exaggerated for clarity. The hyperfine structure is not shown.

hyperfine levels. The hyperfine levels are labeled by F, which is the quantum number of the grand total angular momentum $\vec{F} = \vec{j} + \vec{I}$, and takes values between $|j - I|$ and $|j + I|$.

There are many studies of the energy levels of PO and the potential energy curves of the ground and excited electronic states. We will briefly review, in chronological order, the ones that are relevant to our work here. Verma et al. [13] and Zaidi et al. [14] using the results of high-resolution electronic spectroscopy obtained values of the spin-orbit constant, A, and studied its vibrational dependence for vibrational states $v = 0$ to $v = 11$. Kawaguchi et al. [15] used microwave and far-infrared laser magnetic resonance spectroscopy to study the rotational levels in $v = 0$. Butler et al. [16] employed tunable infrared diode laser spectroscopy to study the $v = 1$ state. Kanata et al. [7] used the Stark effect to determine the dipole moment of PO to be 1.88(7) D in the $^2\Pi_{3/2}$, j = 4.5-6.5 levels. Qian et al. [17] used infrared absorption spectroscopy in the PO fundamental band observed many transitions in the P- and R-branch. Qian [18] used an effective Hamiltonian to fit these transitions along with the previously obtained microwave data, and obtained improved values of the molecular constants especially for $v = 1$. The most recent work was done by Bailleux et al. [19] who obtained millimeter-wave transitions in excited vibrational states up to $v = 7$ and obtained the most recent values of the PO molecular constants. Moussaoui et al. [20] have reviewed previous work on PO in its ground electronic state. From a theoretical point of view, ab initio potential energy curves of the ground [21] and excited [22, 23] electronic states have been presented.

In order to simulate the spectra of PO in the interstellar and circumstellar media, accurate collisional rate coefficients and radiative rates are necessary. Indeed, because of the low densities, collisions compete with radiative processes in altering populations in molecular energy levels. Regarding collisions, the predominant collision partners in the cold interstellar and circumstellar gas are the He atom and the molecular hydrogen [24]. Inelastic rate coefficients for the He + PO system require demanding calculations because PO is an open-shell molecule with a low rotational constant, B. We present here the first *ab initio* intermolecular potential energy surface (PES) for this system. Using this PES and quantum scattering calculations, we also present rotational and hyperfine cross sections. The paper is organized as follows: Section II presents the ab initio calculations, and the analytical fit of the PES obtained. In Section III, the details of the scattering calculations are presented, and the theoretical inelastic integral cross sections (ICS) and differential cross sections (DCS) obtained are discussed and compared with similar systems. Conclusions and future outlook are also presented.

II. PO(X)– HE POTENTIAL ENERGY SURFACES

A. *Ab initio* calculations

When the PO($X^2\Pi$) radical interacts with a spherical structureless target, the doubly-degenerate Π electronic state is split into two states, one of A' symmetry and one of A'' symmetry. The PO–He "rigid rotor" (i.e. the internuclear distance of PO is kept fixed) PESs are described by the two Jacobi coordinates: R, the distance from the centre of mass of PO molecule to the He atom, and θ, the angle between $\vec{R}$ and the PO bond axis $\vec{r}$, with $\theta = 0°$ corresponding to collinear He–OP. The intermolecular bond distance of PO was frozen at its experimental equilibrium values ($r_{\rm PO}$ = 2.789 bohr [25]).

Ab initio calculations of the PESs of He–PO($X^2\Pi$) van der Waals complexes being in A' and A'' electronic states were carried out at the partially spin-restricted coupled cluster with single, double and perturbative triple excitations [UCCSD(T)] [26, 27] level of theory using MOLPRO 2010 package [28]. In order to determine the interaction potential, $V(R, \theta, r_{\rm PO})$, the basis set superposition error (BSSE) was corrected at all geometries using the Boys and Bernardi counterpoise scheme [29]:

$$V(R,\theta,r_{\rm PO}) = E_{\rm PO-He}(R,\theta,r_{\rm PO}) - E_{\rm PO}(R,\theta,r_{\rm PO}) - E_{\rm He}(R,\theta,r_{\rm PO}) \quad (1)$$

where the energies of the PO and He monomers are computed in a full basis set of the complex.

For all three atoms, we used the standard correlation-consistent polarized valence-triple-zeta basis sets of Dun-

ning [30] (cc-pVTZ) augmented with the diffuse functions (aug-cc-pVTZ) [31]. This basis set was further augmented by bond functions placed at mid-distance between the He atom and the PO centre of mass. Such approach is expected to lead to reliable PESs that can safely be used for astrophysical applications [32].

The calculations were carried out for θ angle values from 0° to 180° in steps of 10°. R-distances were varied from 3.0 to 50.0 a_0, yielding 41 points for each angular orientation.

B. Analytical representations

For dynamical calculations, an analytical expansion of the potentials is required. For both A' and A'' surfaces, we have adopted the fitting procedure described by Werner et al. [33] for the CN−He complex. Such a procedure leads us to generate the $V(R,\theta)$ numerical expansion routine which is implemented later in the dynamical computations code:

$$V(R,\theta) = \sum_{l=1}^{L} A_{ln}(R) d_{m,0}^{l+m-1}(cos\theta) \qquad (2)$$

where the $d_{m,0}^{l+m-1}$ are the reduced rotation matrix elements of Wigner, and L represents the total number of the *ab initio* angles. Two-dimensional cuts of the A' and A'' PES for $r = r_e$ are shown in Fig. 2. The minimum of $V_{A'}(R,\,\theta)$ is -28.60 cm^{-1} at ($R = 6.90\,a_0$, $\theta = 63°$), and of $V_{A''}(R,\theta)$ is -29.01 cm^{-1} at ($R = 6.90\,a_0$, $\theta = 107°$). The shape of the two PESs are quite different. The A'' PES seems to present a relatively higher anisotropy with respect to PO rotation contrarily to the A' PES that significantly vary with the θ angle.

In the scattering calculations, it is more convenient [34] to use the average

$$V_{\rm sum} = \frac{1}{2}\left(V_{A''} + V_{A'}\right) \qquad (3)$$

and the half-difference

$$V_{\rm diff} = \frac{1}{2}\left(V_{A''} - V_{A'}\right) \qquad (4)$$

of these two potential energy surfaces. In the pure Hund's case (a) limit, $V_{\rm sum}$ is responsible for inducing inelastic collisions within a given spin-orbit manifold, and $V_{\rm diff}$ for inducing inelastic collisions between the $^2\Pi_{1/2}$ and $^2\Pi_{3/2}$ spin-orbit manifolds. The plots of $V_{\rm sum}$ and $V_{\rm diff}$ are presented in Fig. 3. The PESs are available from the authors upon request.

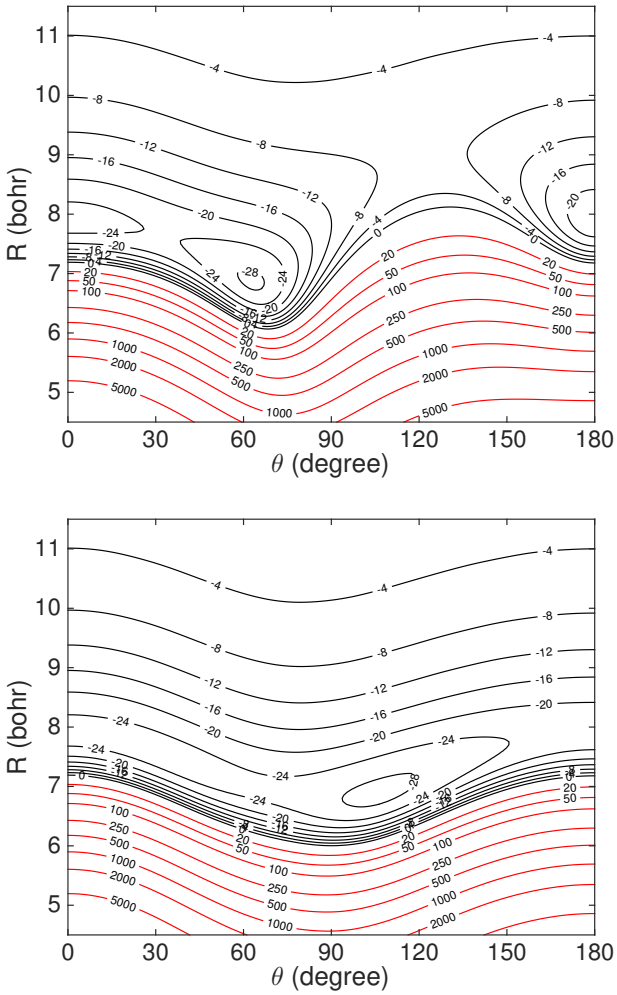

FIG. 2: Contour plots of PO(X)–He adiabatic A'' (upper panel), and A' (lower panel) UCCSD(T) potentials. Energy is in cm^{-1}. Red contour lines represent repulsive interaction energies.

III. RESULTS

A. Scattering calculations

Close-coupling quantum scattering calculations were performed using the newly constructed PES. The calculations were carried out using HIBRIDON program, [35] which provided integral and differential cross sections. Details on how to obtain the nuclear spin free $S^J(F_i j\varepsilon l; F_i' j'\varepsilon' l')$ scattering matrices between the PO rotational levels followed the standard formalism for collisions of diatomic open-shell molecules with atoms [34, 36]. In the above notation, F_i denotes the spin-orbit manifold, l the orbital angular momentum quantum numbers, and J the total angular momentum ($\vec{J} = \vec{j} + \vec{l}$). The symbols ε, ε' label the Λ-doublet level which can be

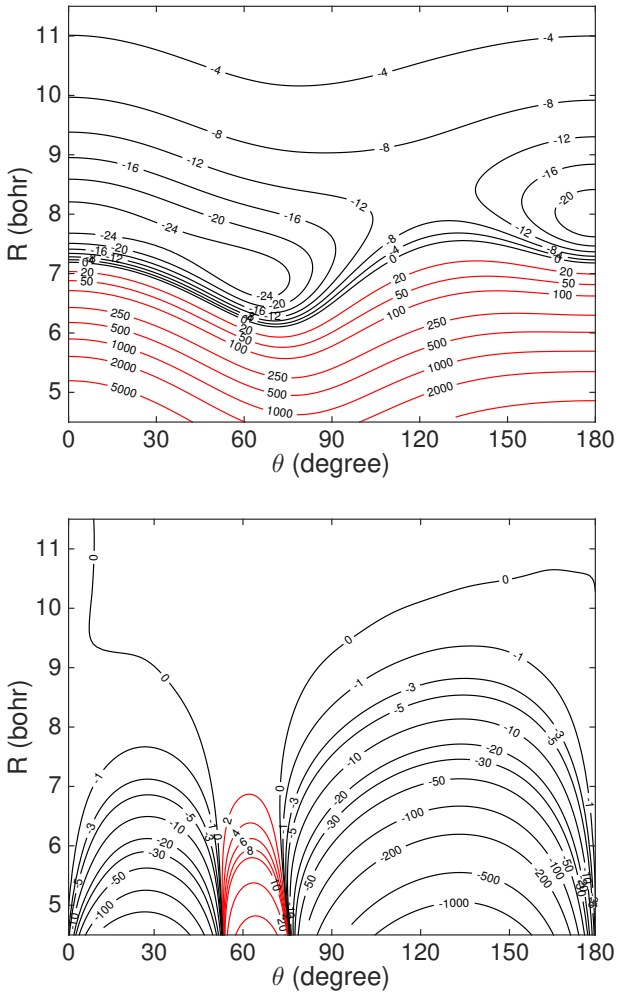

FIG. 3: Contour plots of PO(X)–He diabatic $V_{\rm sum}$ (upper panel), and $V_{\rm diff}$ (lower panel) UCCSD(T) potentials. Energy is in $\rm cm^{-1}$. Red contour lines represent repulsive interaction energies.

either e or f.

The Hamiltonian for the PO considered the PO rotation, spin-orbit coupling and Λ-doublet splitting using the PO rotation constant $B = 7.332237 \times 10^{-1}\,\rm cm^{-1}$, the spin-orbit coupling constant $A = 224.01\,\rm cm^{-1}$, and Λ-doubling parameters $p = 6.2782 \times 10^{-3}\,\rm cm^{-1}$ and $q = -2.227 \times 10^{-5}\,\rm cm^{-1}$ [19]. The reduced mass for He-PO was $\mu = 3.68829228$ amu. In the scattering calculations reported here, the hyperfine structure of PO was not explicitly taken into account, and the value of the PO spin-orbit constant was assumed to be independent of the intermolecular separation. The maximum value of the total angular momentum quantum number, $J_{\rm tot}$, was 240, and all the channels up to a maximum value of the PO rotational quantum number, $j_{\rm max} = 36$, were included. Close-coupling quantum calculations were performed on a grid of energies up to a total energy of $960\,\rm cm^{-1}$. The energy steps were $0.5\,\rm cm^{-1}$ between $0.5\,\rm cm^{-1}$ and $100\,\rm cm^{-1}$, $1\,\rm cm^{-1}$ between 100 and $500\,\rm cm^{-1}$, $2\,\rm cm^{-1}$ between $502\,\rm cm^{-1}$ and $960\,\rm cm^{-1}$. Hyperfine cross sections can be obtained from the rotational scattering, S-matrices using the recoupling method [34, 37] assuming that the hyperfine levels are degenerate. The total angular momentum J_T of the colliding system including nuclear spin is given by $J_T = J + I$. Hyperfine cross sections for transitions from $F_i j \varepsilon F$ to $F_i' j' \varepsilon' F'$ can be obtained from the following equation [37]:

$$\sigma_{F_i j \varepsilon F \to F_i' j' \varepsilon' F'} = \frac{\pi}{k^2_{F_i j \varepsilon F}} (2F'+1) \sum_{J_T} (2J_T+1) \sum_{ll'} |\delta_{F_i F_i'} \delta_{jj'} \delta_{ll'} \delta_{FF'} - S^{J_T}(F_i j \varepsilon F l; F_i' j' \varepsilon' F' l')|^2 \tag{5}$$

where $S^{J_T}(F_i j \varepsilon F l; F_i' j' \varepsilon' F' l')$ denotes the S-matrix for a total angular momentum J_T and $k^2_{F_i j \varepsilon F}$ is the initial wavevector.

The S^{J_T}-matrix elements can be obtained from the nuclear spin-free S^J-matrix by the equation [37]:

$$S^{J_T}(F_i j \varepsilon F l; F_i' j' \varepsilon' F' l') = \sum_J \left[(2F+1)(2F'+1)\right]^{1/2} (2J+1) \times (-1)^{F+F'+l+l'-2J_T} \begin{Bmatrix} l & j & J \\ I & J_T & F \end{Bmatrix} \times \begin{Bmatrix} l' & j' & J \\ I & J_T & F' \end{Bmatrix} S^J(F_i j \varepsilon l; F_i' j' \varepsilon' l') \tag{6}$$

B. Integral cross sections

First, we focus on the results ignoring the hyperfine structure of the PO target. Integral cross sections (ICSs) have been obtained for transitions up to $j = 7.5$. The integral cross sections obtained for He + PO($^2\Pi_{1/2}, v = 0, j = 0.5$) collisions at $E_{\rm col} = 500\,\rm cm^{-1}$ are shown in Fig. 4 for the spin-orbit conserving (upper panel) and the spin-orbit changing (lower panel) collisions, resolved into initial and final Λ-doublet levels. As also observed in He + NO [38], the ICSs exhibit an oscillatory structure as a function of the final rotational state. We note that the ICSs for spin-orbit conserving are significantly larger than for spin-orbit changing. This is similar, albeit to a much more pronounced way, to the corresponding ratios in He–NO($^2\Pi_{1/2}, v = 0, j = 0.5$) at around $1200\,\rm cm^{-1}$ in ref. [39]. Given that PO is a Hund's case (a) open-shell diatomic, spin-orbit collisions are governed by the $V_{\rm sum}$ potential, and the spin-orbit changing collisions occur on the $V_{\rm diff}$. The $V_{\rm diff}$ in He-PO and in He-NO are mostly negative and in absolute size smaller than $V_{\rm sum}$ as shown in Fig. 3 in this paper and in Fig. 1 in ref. [39]. This difference in the underlying PESs explains the difference in the ICSs for collisions into the two spin-orbit manifolds.

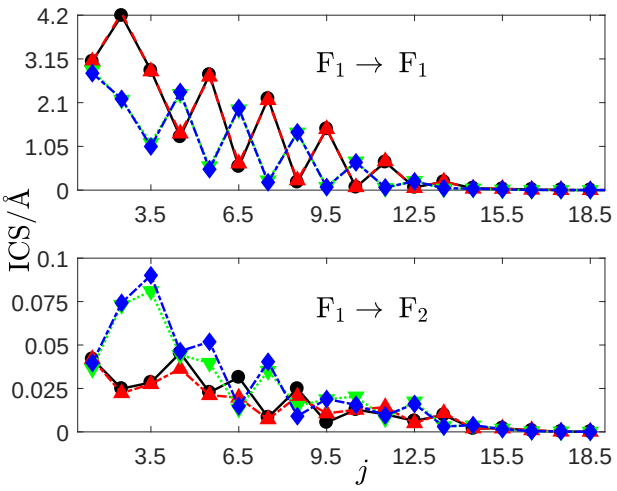

FIG. 4: Close-coupling quantum mechanical state-to-state ICSs for PO($^2\Pi_{1/2}, v = 0, j = 0.5$) scattered by He at a collision energy of 500 cm^{-1}. The spin-orbit conserving ICSs versus final rotational level j are shown in the upper panel, and the spin-orbit changing ICSs are in the lower panel. ICS for $e \to e$ are shown in black • (solid line), $f \to f$ are shown in red ▲ (dashed line), $e \to f$ are shown in green ▼ (dotted line), and $f \to e$ are shown in blue ♦ (dashed-dotted line).

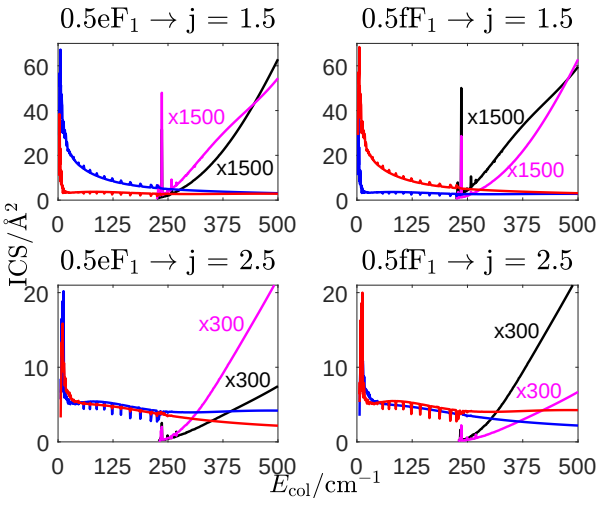

FIG. 5: Close-coupling quantum mechanical state-to-state excitation functions for PO($^2\Pi_{1/2}, v = 0, j = 0.5$) scattered by He. The initial spin-orbit state and Λ-doublet component, and the final j are shown in the title of the graphs. The final products are shown: eF$_2$ (black), fF$_2$ (purple), eF$_1$ (blue) and fF$_1$ (red).

The spin-orbit constant of PO is around twice those of NO, and this can explain the greater ratio of $F_1 \to F_1$ versus $F_1 \to F_2$ in the He-PO case.

In the limit of a pure Hund's case (a), the values of the ICSs for $e \to e$ and $e \to f$ collisions should be identical to those for $f \to f$ and $f \to e$, respectively [40]. For He + NO $F_1 \to F_1$ collisions the sizes of the ICSs were: $e \to f \geq f \to e$, $f \to f \geq e \to e$; the reverse trend observed for the spin-orbit-changing transitions (see Fig. 4 in ref. [39]). In the He–PO case, we see a similar effect mostly for the spin-orbit changing collisions where $f \to e \geq e \to f$, $e \to e \geq f \to f$ for low rotational excitation. However, there are some exceptions for higher final PO rotational levels.

State-to-state inelastic cross sections for collisions He + PO(F_1, $v = 0, j = 0.5e/f$) to He + PO(F_1/F_2, $v = 0, j = 1.5-2.5e/f$) levels at various collision energies up to 500 cm^{-1} are shown in Fig. 5. At collision energies up to 400 cm^{-1} many sharp spikes appear. This is common in inelastic scattering and is usually due to either Feshbach or shape resonances. Feshbach resonance may arise due to excitation of the He-PO complex to a level which is energically accessible because of the attractive well but is asymptotically closed. Shape resonances may arise because of tunneling through the centrifugal energy barrier. The analysis of resonances is beyond the scope of this article. As shown in Fig. 5, the cross sections for spin-orbit conserving collisions are often between 300 and 1500 times larger than those of spin-orbit changing collisions.

C. Differential cross sections

Gijsbertsen et al. [38, 41, 42] studied collisions of He/D_2 + NO(X) collisions, and showed that the differential cross sections (DCSs) for scattering into pairs of levels with the same value of $n = j' - \varepsilon\varepsilon'/2$ had similar shapes. For example, for spin-orbit conserving transitions in the lower spin-orbit state, the final rotational levels $j = 2.5e$ and $j = 3.5f$ had $n = 3$, and showed similar DCS. In a theoretical study of He + NO collisions, Kłos et al. [43] divided the inelastic collisions into two categories. The first one, which was applicable for low Δj transitions, could be described by a direct scattering and the similarity in ICS and DCS reflected the symmetry properties of the potential matrix elements that coupled different initial and final levels. In the second category, which was applicable for high Δj, the transitions could be considered to occur via tiers of 'virtual' states. In those cases, the similarity in ICS and DCS reflected the symmetry properties of the matrix elements that coupled initial and 'virtual' states, and of the matrix elements that coupled 'virtual' and final states. Kłos et al. [43] showed that $\Delta j = n, e \to e$ and $\Delta j = n-1, e \to f$ transitions were both directly coupled by a single term in the potential, the $V_{n0}(R)$. Thus, transitions ending to 'adjacent parity pairs', i.e. levels with the same total parity, $p = \epsilon'(-1)^{(j'-1/2)}$, and common value of $n = j' - \epsilon\epsilon'/2$, show similar DCSs. The calcu-

lated DCS for He + PO($^2\Pi_{1/2}, v = 0, j = 0.5$) transitions at a collision energy of 500 cm^{-1} are shown in Fig. 6 for the spin-orbit conserving collisions, and in Fig. 7 for the spin-orbit changing collisions in increasing 'adjacent parity pairs' n-index.

As discussed by Aoiz et al. [39] on a study of the similar He–NO system, the DCS exhibits narrow glory-type diffraction oscillations at low scattering angles. These are due to interferences of 'trajectories' with large angular momenta that pass through the long-range part of the PES and emerge close to the forward direction. Quite often, the experimental resolution is too low to resolve these oscillations [38]. The DCSs for $F_1 \rightarrow F_1$ (Fig. 6 are significantly more forward than those for $F_1 \rightarrow F_2$ (Fig. 7. At high Δj, the DCS of spin-orbit conserving and spin-orbit changing transitions become more similar possibly because the spin-orbit states become mixed.

Spotting rotational rainbows (i.e. maxima) in DCSs has been a topic of particular interest in the last years [39, 43]. Finding rotational rainbows is not always a simple task, because they depend on the initial and final level, the collision energy and the initial population [44]. It is indeed very important to select the initial Λ-doublet level because the DCSs from the two Λ-levels can be very different. The most common method of selecting a Λ-level is using hexapole electrostatic fields, where only the f initial level of the lowest rotational level is selected. Based on the theoretical predictions in Fig. 6, we would propose the $n = 5 - 7$ transition for the experimental observation of the single rotational rainbow. Regarding the spin-orbit changing transitions, we would propose the $n = 3$ for the double rotational rainbow.

D. Hyperfine cross sections

State-to-state hyperfine cross sections for collisions of PO(X $^2\Pi_{1/2}, v = 0, j = 0.5e, F = 1$) and He are shown in Fig. 8. The final states are the almost isoenergetic $j = 2.5e/f, F = 2, 3$, and the transition corresponds to $\Delta j = 2$. Numerous spikes appear at collision energies up to around 300 cm^{-1}, and the widths of the spikes become larger at higher collision energies. The energy differences between all the four final hyperfine levels are very small compared with the available collision energies. Therefore, any differences in the cross sections among the final levels should arise from the matrix elements responsible for the rotational transitions, and the recoupling method employed for the hyperfine-resolved cross sections. As shown in Fig. 5, for collisions starting from $0.5eF_1$, the rotational cross section for the eF_1 final level is larger than that for the fF_1 level at high collision energies. This trend is, of course, observed in Fig. 8, if one compares the average of the hyperfine-resolved cross sections into $j = 2.5e, F = 2, 3$ with the average of the $j = 2.5f, F = 2, 3$. As shown in Fig. 8, for the e final levels, the hyperfine cross sections are higher for those with higher F quantum number, and the reverse is true for the f final levels. This trend is not only for the final $j = 2.5$ level, but it is general for the final $j = 2.5 - 7.5$ levels with few exceptions at low collision energies. We note that when the initial level is $j = 0.5e, F = 0$, the opposite trend is observed, i.e. for the final eF_1 levels, the hyperfine cross sections are higher for lower F quantum numbers.

We now turn our attention to the hyperfine cross sections for transitions within a Λ-doublet. We will follow closely the approach employed in ref. [37] in the study of hyperfine propensities in He + OH Λ-doublet changing collisions. For each Λ-doublet level, there are two possible hyperfine quantum numbers. We will refer to them as $F_{\rm max}$ and $F_{\rm min}$, with $F_{\rm max} > F_{\rm min}$. We emphasize that the subscripts max and min refer to the relative magnitude of the grand angular momentum quantum number and not to the energy. For an $f \rightarrow e$ Λ-doublet changing collision, there are four possible transitions: $F_{\rm max} \rightarrow F_{\rm max}$, $F_{\rm max} \rightarrow F_{\rm min}$, $F_{\rm min} \rightarrow F_{\rm max}$, and $F_{\rm min} \rightarrow F_{\rm min}$. As examined in ref. [37], the cross sections should have higher values in the following order: $F_{\rm max} \rightarrow F_{\rm max} \geq F_{\rm min} \rightarrow F_{\rm min} > F_{\rm min} \rightarrow F_{\rm max} \geq F_{\rm max} \rightarrow F_{\rm min}$. The calculated hyperfine cross sections for the $1.5f \rightarrow 1.5f$ collisions in the $^2\Pi_{3/2}$ state are shown in Fig 9, and follow this prediction.

IV. DISCUSSION AND CONCLUSIONS

The interstellar gas phase chemistry of phosphorus remains poorly known because phosphorus-bearing species are very toxic and difficult to handle with in laboratory experiments. Despite this limitation, the comparison of astronomical observations of species such as PO and PN with models of the chemistry of phosphorus in the ISM can provide important constraints to the dominant formation/destruction routes of these phosphorus-bearing molecules.

Recent observations of PO and PN in star-forming regions have revealed that PO is more abundant than PN [10, 11]. At high-temperatures, such as those found in shocked regions associated with molecular outflows driven by young protostars, the formation of PN proceeds via the reaction N + PO → PN. This reaction is very sensitive to the amount of atomic N present in the gas phase, and therefore, the fact that the PO/PN abundance ratio is ∼2-3 suggests that atomic N cannot be the main nitrogen reservoir in star-forming regions. This can occur, however, for a long-lived pre-stellar phase where atomic N is almost completely frozen onto the surface of dust grains [11].

Unlike PN for which collisional coefficients with He are available [45], the measurements of molecular abundances of PO are subject to large uncertainties due to the lack of any collisional coefficients calculated for this molecule. Indeed, while previous studies have determined the abundance of PN using non-local thermodynamic equilibrium (non-LTE) radiative transfer models,

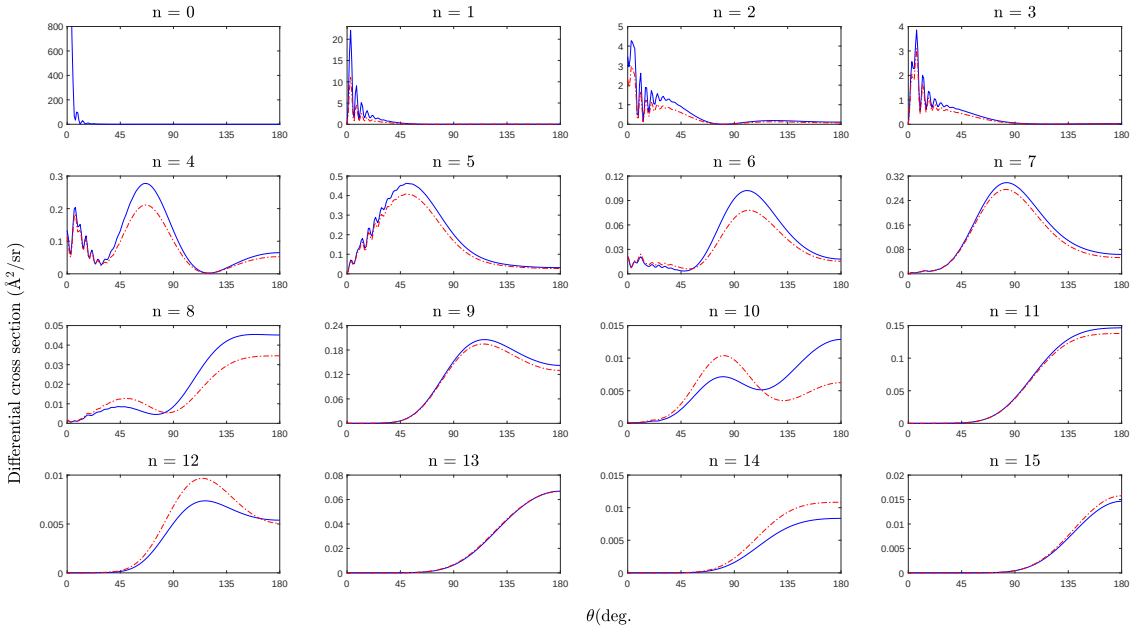

FIG. 6: Close-coupling quantum mechanical state-to-state differential cross sections (DCSs) for spin-orbit conserving $\mathrm{PO}(^2\Pi_{1/2}, v = 0, j = 0.5f)$ + He transitions at a collision energy of 500 cm^{-1}. Transitions into $f\mathrm{F}_1$ and $e\mathrm{F}_1$ are depicted by blue, solid lines and red, dashed-dotted lines, respectively. The n-index of the 'adjacent parity pair' is shown in the title of each graph.

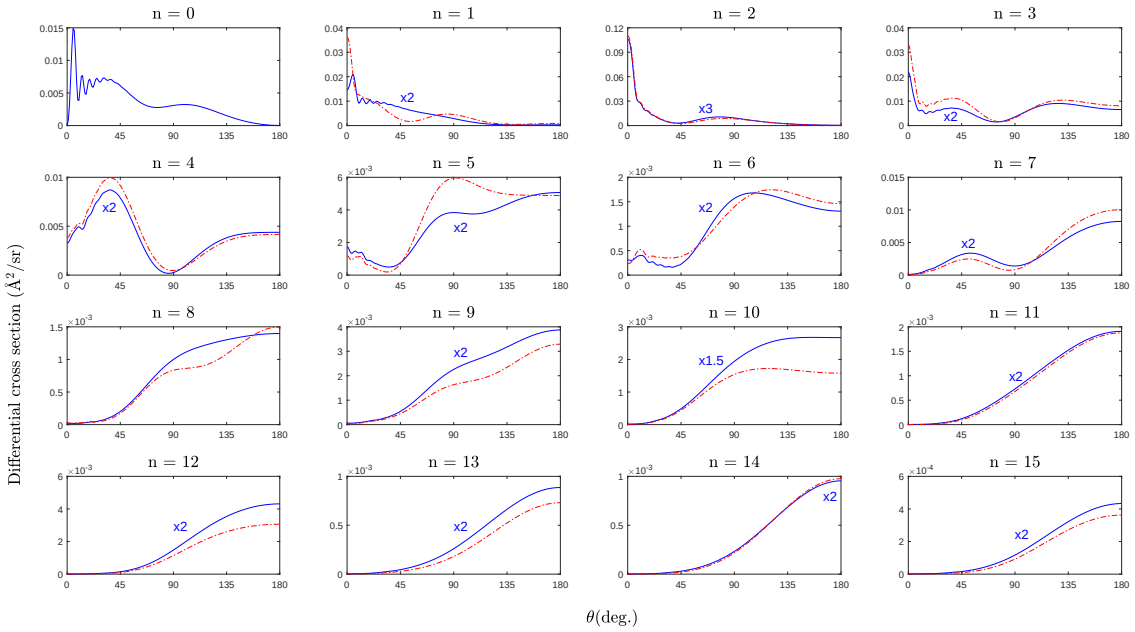

FIG. 7: Close-coupling quantum mechanical state-to-state differential cross sections (DCSs) for spin-orbit changing $\mathrm{PO}(^2\Pi_{1/2}, v = 0, j = 0.5f)$ + He transitions at a collision energy of 500 cm^{-1}. Transitions into $f\mathrm{F}_2$ and $e\mathrm{F}_2$ are depicted by blue, solid lines and red, dashed-dotted lines, respectively. The n-index of the 'adjacent parity pair' is shown in the title of each graph.

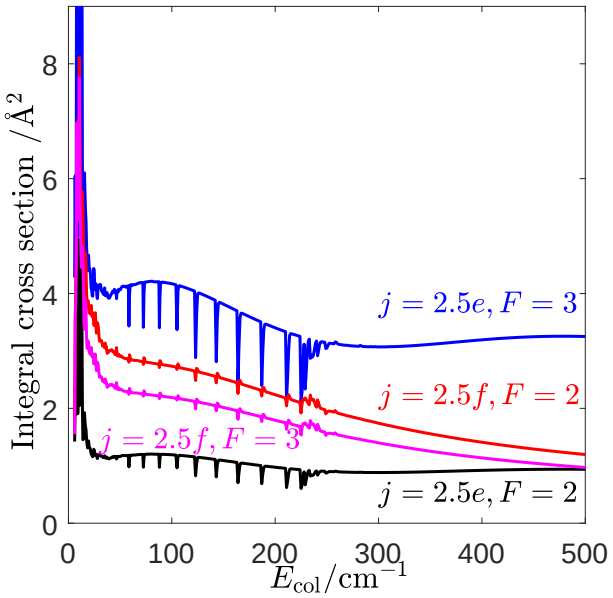

FIG. 8: State-to-state hyperfine cross sections for collisions of PO(X $^2\Pi_{1/2}, v = 0, j = 0.5e, F = 1$) and He. The results for final levels in the $j = 2.5$ for spin-orbit conserving collisions are shown. The final j, ε, F are shown in the graph.

this is not the case for PO for which a simple (and probably inaccurate) LTE approximation has been considered [10, 11]. Therefore, calculations of the collisional rate coefficients for the PO-He system, will allow accurate estimates of the excitation conditions of this molecule in the non-LTE regime, providing important constraints to the actual abundance of this molecule with respect to PN and to the chemistry of this important prebiotic compound in star-forming regions. The complete set of these rate coefficients among channels up to $j = 7.5$ will be available online from the BASECOL [46] and LAMDA [47] databases.

ACKNOWLEDGEMENTS

We acknowledge the financial support from the COST Action CM1401 "Our Astrochemical History". This research utilized Queen Mary's Mid-Plus computational facilities, supported by QMUL Research-IT and funded by EPSRC grant EP/K000128/1. S. M. acknowledges Indigo Dean for very useful discussions. I.J.-S. acknowledges the financial support received from the STFC through an Ernest Rutherford Fellowship (proposal number ST/L004801).

[1] M. Asplund, N. Grevesse, A. J. Sauval, and P. Scott, Annu. Rev. Astron. Astrophys. **47**, 481 (2009).
[2] E. Masia, Chem. Soc. Rev. **34**, 691 (2005).
[3] B.-C. Koo, Y.-H. Lee, D.-S. Moon, S.-C. Yoon, and J. C. Raymond, Science **342**, 1346 (2013).
[4] M. Jura and D. G. York, Astrophys. J. **219**, 861 (1978).
[5] M. Agúndez, J. Cernicharo, and M. Guélin, Astrophys. J. Lett. **790**, L27 (2007).
[6] M. Agúndez, J. Cernicharo, L. Decin, P. Encrenaz, and D. Teyssier, Astrophys. J. Lett. **790**, L27 (2014).
[7] H. Kanata, S. Yamamoto, and S. Saito, J. Mol. Spectrosc. **131**, 89 (1988).
[8] E. D. Tenenbaum, N. J. Woolf, and L. M. Ziurys, Astrophys. J. Lett. **666**, 29 (2007).
[9] E. De Beck, T. Kamiński, N. A. Patel, K. H. Young, C. A. Gottlieb, K. M. Menten, and L. Decin, Astron. Astrophys. **558**, A132 (2013).
[10] V. M. Rivilla, F. Fontani, M. T. Beltrán, A. Vasyunin, P. Caselli, J. Martín-Pintado, and R. Cesaroni, Astrophys. J. **826**, 161 (2016).
[11] B. Lefloch, C. Vastel, S. Viti, I. Jimenez-Serra, C. Codella, L. Podio, C. Ceccarelli, E. Mendoza, J. R. D. Lepine, and R. Bachiller, Mon. Not. R. Astron. Soc. **462**, 3937 (2016).
[12] T. Aota and Y. Aikawa, Astrophys. J. Lett. **761**, 74 (2012).
[13] R. D. Verma and S. R. Singhal, Can. J. Phys. **53**, 411 (1975).
[14] H. R. Zaidi and R. D. Verma, Can. J. Phys. **53**, 420 (1975).
[15] K. Kawaguchi, S. Saito, and E. Hirota, J. Chem. Phys. **79**, 629 (1983).
[16] J. E. Butler, K. Kawaguchi, and E. Hirota, J. Mol. Spectrosc. **101**, 161 (1983).
[17] H. B. Qian, P. B. Davies, and P. A. Hamilton, J. Chem. Soc. Faraday Trans. **91**, 2993 (1995).
[18] H. B. Qian, J. Mol. Spectrosc. **174**, 599 (1995).
[19] S. Bailleux, M. Bogey, C. Demuynck, Y. Liu, and A. Walters, J. Mol. Spectrosc. **216**, 465 (2002).
[20] Y. Moussaoui, O. Ouamerali, and G. R. De Maré, J. Mol. Spectrosc. **174**, 599 (2003).
[21] A. Metropoulos, A. Papakondylis, and A. Mavridis, J. Chem. Phys. **119**, 5981 (2003).
[22] J. F. Sun, J. M. Wang, and D. H. Shi, Int. J. Quantum Chem. **112**, 672 (2012).
[23] H. Liu, D. Shi, J. Sun, and Z. Zhu, J. Quant. Spectrosc. Radiat. Transfer **121**, 9 (2013).
[24] E. Roueff and F. Lique, Chem. Rev. **113**, 8906 (2013).
[25] K. P. Huber and G. Herzberg, *Molecular Spectra and Molecular Structure. IV. Constants of Diatomic Molecules* (Van Nostrand Reinhold, New York, 1979).
[26] C. Hampel, K. A. Peterson, and H.-J. Werner, Chem. Phys. Lett. **190**, 1 (1992).
[27] J. D. Watts, J. Gauss, and R. J. Bartlett, J. Chem. Phys. **98**, 8718 (1993).
[28] H.-J. Werner, P. J. Knowles, G. Knizia, F. R. Manby, M. Schütz, P. Celani, T. Korona, R. Lindh, A. Mitrushenkov, G. Rauhut, K. R. Shamasundar, T. B. Adler, R. D. Amos, A. Bernhardsson, A. Berning, D. L. Cooper, M. J. O. Deegan, A. J. Dobbyn, F. Eckert, E. Goll, C. Hampel, A. Hesselmann, G. Hetzer, T. Hrenar,

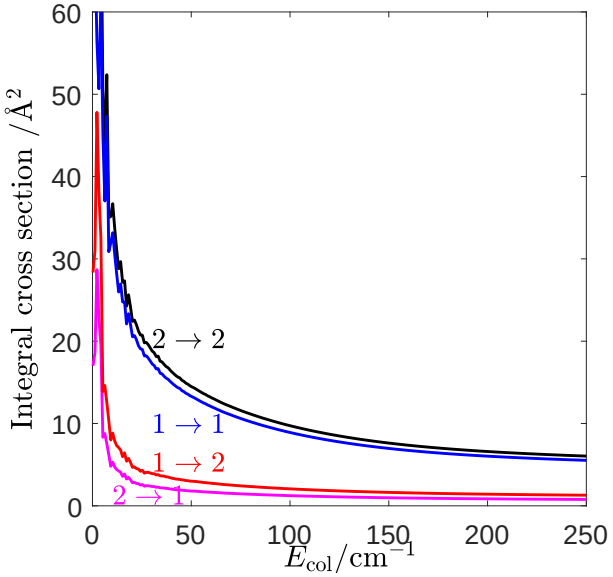

FIG. 9: State-to-state hyperfine cross sections for collisions of PO(X $^2\Pi_{3/2}, v = 0, j = 1.5f$) and He. The results for final levels in the $j = 1.5e$ for spin-orbit conserving collisions are shown. The initial and final F are shown in the graph.

G. Jansen, C. Köppl, Y. Liu, A. W. Lloyd, R. A. Mata, A. J. May, S. J. McNicholas, W. Meyer, M. E. Mura, A. Nicklass, D. P. O'Neill, P. Palmieri, K. Pflüger, R. Pitzer, M. Reiher, T. Shiozaki, H. Stoll, A. J. Stone, R. Tarroni, T. Thorsteinsson, M. Wang and A. Wolf, *MOLPRO, version 2010.1*, a package of *ab initio* programs, 2010, see http://www.molpro.net.

[29] S. F. Boys and F. Bernardi, Mol. Phys. **19**, 553 (1970).

[30] T. H. Dunning, J. Chem. Phys. **90**, 1007 (1989).

[31] R. A. Kendall, T. H. Dunning, and R. J. Harrison, J. Chem. Phys. **96**, 6796 (1992).

[32] F. Lique, A. Spielfiedel, M.-L. Dubernet, and N. Feautrier, J. Chem. Phys. **123**, 134316 (2005).

[33] H.-J. Werner, B. Follmeg, and M. H. Alexander, J. Chem. Phys. **89**, 3139 (1988).

[34] M. Alexander, Chem. Phys. **92**, 337 (1985).

[35] The HIBRIDON package (version 4.4) was written by M. H. Alexander, D. E. Manolopoulos, H.-J. Werner, B. Follmeg, and P. Dagdigian with contributions by D. Lemoine, P. F. Vohralik, G. Corey, R. Gordon, B. Johnson, T. Orlikowski, A. Berning, A. Degli-Esposti, C. Rist, B. Pouilly, J. Kłos, Q. Ma, G. van der Sanden, M. Yang, F. de Weerd, S. Gregurick, and F. Lique, http://www2.chem.umd.edu/groups/alexander/.

[36] Y. Kalugina, F. Lique, and S. Marinakis, Phys. Chem. Chem. Phys. **16**, 13500 (2014).

[37] S. Marinakis, Y. Kalugina, and F. Lique, Eur. Phys. J. D **70**, 97 (2016).

[38] A. Gijsbertsen, H. Linnartz, G. Rus, A. E. Wiskerke, and S. Stolte, J. Chem. Phys. **123**, 224305 (2005).

[39] F. J. Aoiz, J. E. Verdasco, M. Brouard, J. Kłos, S. Marinakis, and S. Stolte, J. Phys. Chem. A **113**, 14636 (2009).

[40] P. J. Dagdigian, M. H. Alexander, and K. P. Liu, J. Chem. Phys. **91**, 839 (1989).

[41] A. Gijsbertsen, H. Linnartz, and S. Stolte, J. Chem. Phys. **125**, 133112 (2006).

[42] A. Gijsbertsen, H. Linnartz, C. A. Taatjes, and S. Stolte, J. Am. Chem. Soc. **128**, 8777 (2006).

[43] J. Kłos, F. J. Aoiz, J. E. Verdasco, M. Brouard, S. Marinakis, and S. Stolte, J. Chem. Phys. **127**, 031102 (2007).

[44] S. Marinakis, I. L. Dean, J. Kłos, and F. Lique, Phys. Chem. Chem. Phys. **17**, 21583 (2015).

[45] R. Toboła, J. Kłos, F. Lique, G. Chałasiński, and M. H. Alexander, Astron. Astrophys. **468**, 1123 (2007).

[46] Dubernet, M.-L., Alexander, M. H., Ba, Y. A., Balakrishnan, N., Balança, C., Ceccarelli, C., Cernicharo, J., Daniel, F., Dayou, F., Doronin, M., Dumouchel, F., Faure, A., Feautrier, N., Flower, D. R., Grosjean, A., Halvick, P., Kłos, J., Lique, F., McBane, G. C., Marinakis, S., Moreau, N., Moszynski, R., Neufeld, D. A., Roueff, E., Schilke, P., Spielfiedel, A., Stancil, P. C., Stoecklin, T., Tennyson, J., Yang, B., Vasserot, A.-M., and Wiesenfeld, L., A&A **553**, A50 (2013).

[47] F. L. Schöier, F. F. S. van der Tak, E. F. van Dishoeck, and J. H. Black, A&A **432**, 369 (2005).